Journal of Theoretical Biology 300 (2012) 242–253

Contents lists available at SciVerse ScienceDirect

Journal of Theoretical Biology

journal homepage: www.elsevier.com/locate/yjtbi

Probabilistic finite element analysis of a craniofacial finite element model

Michael A. Berthaume [a,b], Paul C. Dechow [c], Jose Iriarte-Diaz [d], Callum F. Ross [d], David S. Strait [e], Qian Wang [f], Ian R. Grosse [a,*]

[a] Department of Mechanical & Industrial Engineering, University of Massachusetts, Amherst, USA
[b] Department of Anthropology, University of Massachusetts, Amherst, USA
[c] Department of Biomedical Sciences, Texas A&M Health Science Center Baylor College of Dentistry, Dallas, TX, USA
[d] Organismal Biology and Anatomy, University of Chicago, Chicago, IL, USA
[e] Department of Anthropology, University at Albany, Albany, NY, USA
[f] Division of Basic Medical Sciences, Mercer University School of Medicine, Macon, GA, USA

ARTICLE INFO

Article history:
Received 7 July 2011
Received in revised form
1 December 2011
Accepted 18 January 2012
Available online 27 January 2012

Keywords:
Probabilistic analysis
Finite element analysis
Model validation
Isotropic and orthotropic material properties
Macaca fascicularis

ABSTRACT

We employed a probabilistic finite element analysis (FEA) method to determine how variability in material property values affects stress and strain values in a finite model of a *Macaca fascicularis* cranium. The material behavior of cortical bone varied in three ways: isotropic homogeneous, isotropic non-homogeneous, and orthotropic non-homogeneous. The material behavior of the trabecular bone and teeth was always treated as isotropic and homogeneous. All material property values for the cranium were randomized with a Gaussian distribution with either coefficients of variation (CVs) of 0.2 or with CVs calculated from empirical data. Latin hypercube sampling was used to determine the values of the material properties used in the finite element models. In total, four hundred and twenty six separate deterministic FE simulations were executed.

We tested four hypotheses in this study: (1) uncertainty in material property values will have an insignificant effect on high stresses and a significant effect on high strains for homogeneous isotropic models; (2) the effect of variability in material property values on the stress state will increase as non-homogeneity and anisotropy increase; (3) variation in the *in vivo* shear strain values reported by Strait et al. (2005) and Ross et al. (2011) is not only due to variations in muscle forces and cranial morphology, but also due to variation in material property values; (4) the assumption of a uniform coefficient of variation for the material property values will result in the same trend in how moderate-to-high stresses and moderate-to-high strains vary with respect to the degree of non-homogeneity and anisotropy as the trend found when the coefficients of variation for material property values are calculated from empirical data. Our results supported the first three hypotheses and falsified the fourth.

When material properties were varied with a constant CV, as non-homogeneity and anisotropy increased the level of variability in the moderate-to-high strains decreased while the level of variability in the moderate-to-high stresses increased. However, this is not the pattern observed when CVs calculated from empirical data were applied to the material properties where the lowest level of variability in both stresses and strains occurred when the cranium was modeled with a low level of non-homogeneity and anisotropy. Therefore, when constant material property variability is assumed, inaccurate trends in the level of variability present in modest-to-high magnitude stresses and strains are produced.

When the cranium is modeled with the highest level of accuracy (high non-homogeneity and anisotropy) and when randomness in the material properties is calculated from empirical data, there is a large level of variability in the significant strains (CV=0.369) and a low level of variability in the modest-to-high magnitude stresses (CV=0.150). This result may have important implications with regard to the mechanical signals driving bone remodeling and adaptation through natural selection.

1. Introduction

1.1. Background: FEA in biology

Over the past ten years many researchers in comparative morphology and physical anthropology have adopted finite element analysis (FEA) as a tool to simulate feeding biomechanics

* Corresponding author. Tel.: +1 413 545 1350.
E-mail address: grosse@ecs.umass.edu (I.R. Grosse).

0022-5193/$ - see front matter © 2012 Elsevier Ltd. All rights reserved.
doi:10.1016/j.jtbi.2012.01.031

(Strait et al., 2005; Ross et al., 2011; Dumont et al., 2011; Wood et al., 2011; O'Higgins et al., 2011; Porro et al., 2011; Davis et al., 2011; Berthaume et al., 2010; Rayfield, 2007; Dumont et al., 2005). Finite element models of craniofacial skeletal structures enable researchers to predict the complete stress and strain fields throughout the cranium as a result of loading conditions that simulate orofacial functions, such as mastication or ingestion of mechanically resistant foods, and to test hypotheses regarding craniofacial shape, feeding performance, and behavior (Strait et al., 2005; Ross et al., 2011; Ross et al., 2005).

FEA is a computer-based technique used to solve the governing field equations in continuum mechanics, such as the equations of elasticity. It is widely used by engineers for structural analysis, thermal analysis, fluid flow analysis, and electromagnetic analysis. Initial applications of FEA to biological systems involved relatively simple geometric idealizations of human skeletal structures, such as the femur (Brekelmans et al., 1972; Rybicki et al., 1972). Subsequent improvements in technology enabled geometrically complex tissue structures to be digitally reconstructed from CT scans, opening the door to the application of FEA to a wide variety of biological systems, such as mammalian skulls (Dumont et al., 2005), dinosaur skulls (Rayfield, 2004), alligator skulls (Porro et al., 2011; Metzger et al., 2005; Reed et al., 2011), shark jaws (Wroe et al., 2008), seahorse snouts (Leysen et al., 2010), and blue crab legs (Hecht et al., 2010).

One of the few finite element models of a biological system validated by *in vivo* data is the macaque cranium model developed by Strait et al. (2005) and Ross et al. (2005) to simulate feeding biomechanics. (This model was validated again with additional *in vivo* data gathered from multiple individuals in Ross et al. (2011). Other FE models validated with *in vivo* data include a rat ulna (Kotha et al., 2004) and an alligator cranium (Metzger et al., 2005).) It should be noted that there was a large level of variation in the *in vivo* data that was used to validate the macaque cranium model, and understanding from where that level of variation originated is of particular interest in this study. In their FE model the researchers varied the type of material behavior (isotropic versus orthotropic) and the degree to which material property values vary spatially, i.e. non-homogeneity. This was assessed by dividing the cranium into numerous regions, each of which could be assigned different material property values with different levels of anisotropy. Results from this set of models were then compared to the range of strain values measured *in vivo* on different individuals and collected and published by various researchers. Since most of the data gathered from the simulations fell within the dispersion of the *in vivo* data, the model was considered validated and to be efficient at predicting stress and strain patterns on the surface of a macaque cranium during orofacial function.

Despite such successes, some morphologists have concerns regarding the deterministic nature of finite element models (Grine et al., 2010). This is typically not as much an issue in the engineering world, as considerable effort is expended by engineers to reduce variability in the performance of engineered products by precise control of the product geometry, material property values, and environmental loading conditions (if possible). However, this is not true in the biological world. Material properties of naturally occurring biological structures, such as bone, are inherently variable due to inter-individual variation in sex, age, genetics, and environment (Peterson and Dechow, 2003; Wang and Dechow, 2006; Zapata et al., 2010; Wang et al., 2010). These variations can be manifested through varying degrees of anisotropy and spatial non-homogeneity (Melchers, 1987). Anisotropic material properties of bone are typically accounted for by orthotropic material models, requiring nine independent elastic constants and three principal material directions which are orthogonal to each other (Malvern, 1969). Spatial non-homogeneity requires spatially detailed measures of material properties, which can be accounted for by assigning different material properties to separate regions in a FEM (Strait et al., 2005; Porro et al., 2011; Wang and Dechow, 2006).

Anisotropy and spatial non-homogeneity in bone material properties can produce an increase in spatial variation in stress and strain values across a single model. When combined with variation in material properties of other connective tissues (e.g., sutures (Reed et al., 2011; Wang et al., 2010; Rayfield, 2005)), constraining conditions, and external forces, variation in bone material properties can produce significant variation in model behavior (Porro et al., 2011). The implications of this variation for our understanding of biological morphology through natural selection are only just beginning to be explored.

1.2. Viewing material properties as "random" variables

A parameter whose values are not known precisely due to uncertainty in measurement and/or other factors is considered to be a random or stochastic variable. If the variable is continuous, it may be mathematically modeled by a probability density function, which mathematically defines the probability that the variable will have a specific value. It should be emphasized that randomness in a variable *does not* require that the variable has equal probability to take on any possible value between two extremes. Such a random variable is defined by a uniform distribution—which would be a rather poor representation of a material property value. Instead, distributions such as Gaussian, log normal, or Weibull distribution have been used to model the natural variability observed in mechanical property values for both biological and engineered materials (McElhaney et al., 1970; Hueste et al., 2004). Comparatively, engineered materials tend to have small coefficients of variation due to high levels of control during the production process whereas biological materials can have fairly large coefficients of variations for the reasons alluded to earlier.

We also note that randomness does not necessarily imply a lack of order or structure. Two or more random variables may be correlated, and this correlation imposes a measure of order on the randomness. For example, consider the Youngs moduli of an orthotropic material: E_3, E_2, and E_1. These moduli are defined as the maximum, intermediate, and minimum stiffnesses, respectively, corresponding to three orthogonal directions called principal material directions. From experimental data, normal distributions for the moduli can be gathered and correlation coefficients between them can be determined to increase the likelihood that $E_3 > E_2 > E_1$ (Peterson and Dechow, 2003; Wang and Dechow, 2006).

1.3. Probabilistic analyses in FEA

Here we apply the techniques of probabilistic FEA to determine the variability (or randomness) in various output variables in an FE model of a cranium due to randomness or variability in material property values. We note that in a conventional finite element analysis, approximate solutions are found using differential equations that are deterministic. Deterministic inputs include boundary conditions such as loads and constraints, material properties, and geometry. Deterministic outputs include quantities such as deformation of the specimen and the stress and strain fields. In probabilistic finite element analysis, there are two types of techniques used to generate variability in outputs resulting from the variability in inputs: non-statistical methods and statistical methods (Sudret and der Kiureghian, 2000; Kang, 2005). Non-statistical methods involve perturbation techniques

by introducing analytical functional approximations of the responses about the mean input. The method is computationally efficient but requires significant mathematical extensions to conventional FEA algorithms and has not been fully developed to encompass the breadth of problems that can currently be solved by conventional FEA tools. As a result, it is not found in mainstream commercial FEA tools.

In the statistical approach, (which includes methods such as the Monte Carlo simulation), input parameters are randomized according to prescribed probabilistic distributions (Gaussian, log-normal, etc.) and a sampling algorithm. Each set of values for the random input parameters produces a set of results (i.e. displacement, strain, and stress fields) through deterministic FEA. Post-processing across all results sets yields statistics for output variables (i.e. such as deflection at specific nodes, maximum von Mises stress or strain, or von Mises stress or strain at specific locations in the mesh). The accuracy of output statistics can be improved with increased sampling. Statistical sampling techniques, such as Latin Hypercube Sampling, are often employed over direct Monte Carlo Simulations, to reduce the number of deterministic FEA analyses required, and response surface modeling approaches can also be used to reduce computational costs.

The probabilistic design portion of ANSYS is an implementation of the statistical approach (Reh et al., 2006). It takes into account the natural variability in input variables by applying a predefined statistical distribution to them. The results can be used to answer a number of questions, such as if the input variables are likely to fall within a certain range, how large the range of the output parameters will be, and which input variables are the most strongly correlated to each, individual output variable.

Probabilistic finite element analysis is not new to engineers. It is widely used in reliability-based approaches that predict the probability of a failure of a system (Melchers, 1987; Der Kiureghian and Ke, 1988; Cesare and Sues, 1999; Lewis, 1987). However, applications of probabilistic FEA to biological systems are limited to the biomedical field. Thacker et al. (2000) used probabilistic FEA to estimate the contribution to injury probability of 29 materials and geometry-related parameters of a finite element model of the lower cervical spine. Nicolella et al. (2001) also used probabilistic FEA of a false hip joint to determine the probability of shear and fatigue failure given certain random variables, such as muscle loading patterns and material properties of the cortical and trabecular bone. One probabilistic analysis has been used to study the macaque zygomatic arch (Kupczik et al., 2007).

Because of the limited use of probabilistic finite element analyses on non-human biological systems, one of the primary purposes of this paper is to compare the results of probabilistic analyses to the *in vivo* data used to validate these models. This comparison will help to determine whether or not variability in material properties contributes significantly to strain variability.

1.4. The hypotheses

Four hypotheses are tested in this paper. First, it is hypothesized that variability in bone material property values between individuals will have little effect on moderate-to-high stresses regions and a significant effect on moderate-to-high strains for homogeneous isotropic models. Second, it is hypothesized that the effect of variability in material property values on the stress state will increase as non-homogeneity and anisotropy increase in the material. Third, it is hypothesized that if the first hypothesis is true, then a significant contribution to variation in the *in vivo* shear strain values reported by Strait et al. (2005) and Ross et al. (2011) may be attributed to variation in material property values between individuals. Finally, it is hypothesized that the assumption of a constant coefficient of variation for all the material properties will result in the same trend in the variation in stresses and strains with respect to the degree of non-homogeneity and anisotropy as found when the coefficients of variation for material properties are calculated from empirical data.

The first two hypotheses are based on the observation that the macaque craniofacial skeleton consists predominantly of cortical bone (the total cranium volume was 39,359 mm^3, with 86.5% of the cranium volume being cortical bone, 5.8% being teeth, and 7.7% being trabecular bone) and hence is similar to a single-material structure. In the linear elastic region of material behavior, the stress state for a homogeneous, isotropic single-material structure is independent of Young's modulus, but the strain state is dependent on it (Timoshenko and Goodier, 1970). The volume of the cranium was calculated using an ANSYS APDL command, a different method for calculating volume than was used in Chamoli and Wroe (2011). Also, it should be noted that what Chamoli and Wroe (2011) define as heterogeneous, we define as three region isotropic, which we consider to have a low level of non-homogeneity. Anisotropy and lack of homogeneity violate the conditions for independence of the stress state on Young's modulus. Thus, with increasing anisotropy and lack of homogeneity, we expect increasing variability in bone stresses due to stochastic material property values, particularly with respect to Young's modulus. These hypotheses were tested by comparing the results of the probabilistic analyses to each other.

The third hypothesis could be falsified if variations in strain due to variation in material property values are relatively small compared to the level of variation in strain observed *in vivo*. This would imply that variability due to material property values between individuals is secondary to variations in morphological structure and masticatory loads between individuals. This hypothesis was tested by comparing the results of the probabilistic analyses to the *in vivo* data. The fourth hypothesis will be tested by comparing the results of 3 models that have a constant coefficient of variation of 0.2 applied to them (models 1, 3, and 5, see Table 1) with the results of 3 models that have coefficients of variation applied to them which were calculated from empirical data (models 2, 4, and 6, see Table 1).

2. Materials and methods

2.1. Macaque FE model

The FE model of the macaque cranium used in this study was constructed by Strait et al. (2005). The macaque model, which consists of 379,388 elements and 131,293 nodes, was developed

Table 1
Description of the six models constructed for the simulations.

Physical description of model	CV=0.2 for input variables	CV for input variables based on empirical data	Level of non-homogeneity	Level of anisotropy	Number of random input variables	Number of simulations run
3 Region, isotropic	Model 1	Model 2	Low	Low	6	30
Multiple region, isotropic	Model 3	Model 4	High	Low	38	39
Multiple region, orthotropic	Model 5	Model 6	High	High	143	144

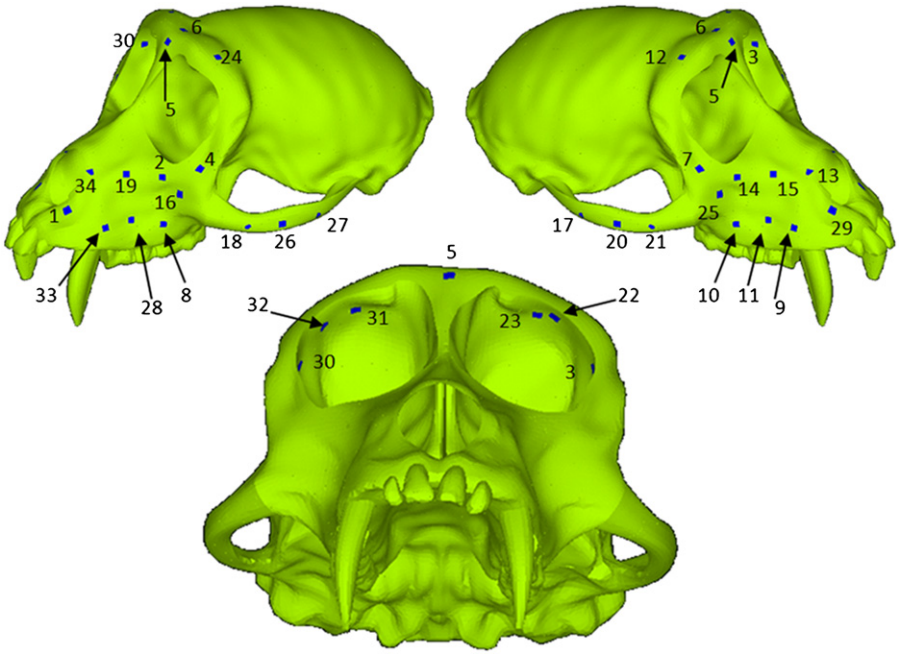

Fig. 1. Locations tested on the cranium are depicted in navy blue. The 34 locations are numbered 1 to 34. 20 of the 34 locations were chosen because they were the same as the 20 sites analyzed in Ross et al. (2011) and the other 14 sites were chosen to extend the total number of locations being tested to the entire anterior portion of the cranium. (For interpretation of the references to color in this figure legend, the reader is referred to the web version of this article.)

in Algor, a commercial FEA program. However, the model was imported into ANSYS APDL 13.0 (see www.ansys.com) using the NASTRAN file format so that ANSYS's probabilistic and sensitivity analysis could be utilized. Subsequently, a number of modifications were made to the model, but the muscle forces remained unchanged. For more information about the construction of the model, please see Strait et al. (2005).

For the isotropic material models tested by Strait et al. (2005), shear modulus, G, Young's modulus, E, and Poisson's ratio, ν, were all specified based on empirical data obtained by (Wang and Dechow, 2006). However, isotropy imposes a relationship between three properties (E, G, and ν) given by the equation:

$$G = E/(2(1+\nu)) \quad (1)$$

Thus, for a true isotropic material model only two of the three properties may be specified independently. In the ANSYS model for isotropic materials, the values of Young's modulus and Poisson's ratio published by Strait et al. (2005) were utilized and the program calculated the shear modulus based on the isotropic relationship of Eq. (1). For orthotropic material behavior, nine elastic constants are required (E_1, E_2, E_3, G_{12}, G_{13}, G_{23}, ν_{12}, ν_{13}, and ν_{23}) which operate in three orthogonal directions (directions 1, 2, and 3) and on three planes (planes 12, 23, and 13), which define the principal material directions and planes within each cranial region.

When the model was constructed by Strait et al. (2005) the teeth were modeled as part of the cortical bone. For purposes of this experiment, the teeth were separated from the cortical bone along the gum line. Because the model was meshed before the teeth were separated, it was not possible to separate out the roots of the teeth or the periodontal ligament (PDL) from the cortical bone.

To simulate the mechanics of biting, an axis of rotation was set up at the temporomandibular joint (TMJ) by constraining a single node at one TMJ in all three coordinate directions and constraining a single node at the other TMJ against anterior–posterior and superior–inferior motion. However, the node was not constrained against medial lateral motion, allowing the cranium to deform laterally (i.e. similar to the "wishboning" seen in mandibles (Hylander and Johnson, 1994)). The nodes on the occlusal surface of the left M[1] were also constrained in the superior–inferior direction to simulate biting down on a hard food item.

2.2. Applying probabilistic analysis to the FEM

A total of six models of the macaque cranium were created and analyzed. Each was assigned a unique set of (a) material properties and/or (b) CVs to the material properties. The analyses for each model consisted of anywhere between 30 and 144 separate deterministic FE simulations using the Probabilistic Design portion of ANSYS APDL 13.0 (see Table 1).

The Probabilistic Design module requires three inputs: a macro code that drives ANSYS, a list of input variables, and a list of output variables. In Probabilistic Design, the macro code is executed N number of times, resulting in N separate finite element analyses. Each deterministic simulation involves a unique set of input parameters that have been designated as random input variables. Statistics for each designated output variable are calculated using the set of N results obtained corresponding to the N deterministic simulations.

In our analyses the random input variables were the set of material properties assigned to each model. Primary output variables were the minimum and maximum principal stresses and strains and the von Mises stresses and strains, exported from the set of nodal solutions at 34 sites on the cranium (all depicted in Fig. 1). The other output variables were ε_x, ε_y, and γ_{xy} normal and shear strains at each site, where these strains are based on a local xyz coordinate system at each of the 34 sites. Each local coordinate system had its origin located at the node being tested and the local xy plane was tangent to the surface of the cranium.

For half of the simulations, material property values (the input variables) were randomized using Gaussian distributions with mean values obtained from empirical data (Wang and Dechow,

[1] Engineering shear strain is twice the tensor shear strain.

2006) and CVs of 0.20. In the other half of the simulations, material property values were randomized using Gaussian distributions with mean values obtained from empirical data (Wang and Dechow, 2006) and standard deviations based on empirical data (Wang and Dechow, 2006). A truncated Gaussian distribution was assigned to Poisson's ratio so it never exceeded 0.4999. (Values larger than 0.5 violate fundamental thermodynamic principles and are not allowed in the theory of elasticity.)

A Monte Carlo simulation with Latin hypercube sampling was used as a method of choosing the values for the random inputs (Olsson and Sandberg, 2002). When Latin hypercube sampling is used in conjunction with a Monte Carlo simulation, an accurate statistical distribution can be obtained while running fewer simulations. (For more information about Monte Carlo simulations with Latin hypercube sampling and how it is used in FEA, please refer to Olsson and Sandberg (2002)) The minimum number of simulations that needed to be run, N, were $N=n+1$ where n is the number of input variables. N cannot be less than 30 in order to permit a normal distribution for the output variables. Because of this, 30 simulations were used to randomize input parameters for models 1 and 2, 39 simulations were used in models 3 and 4, and 144 simulations were used in models 5 and 6 (see Table 1). The minimum number of simulations was used in each Monte Carlo simulation because running a total of over 400 FEA simulations back to back can be costly in terms of computer time and memory. After the analyses were completed, postprocessing in ANSYS provided the values of the output parameters for each simulation and statistical analyses were conducted to calculate the maximum shear strain on the surface of the cranium at each site for comparison to *in vivo* data (Ross et al., 2011).

2.3. Comparing the results to in vivo data

Simulation results were compared to the *in vivo* data gathered on macaques and compiled in Strait et al. (2005) and Ross et al. (2011). Graphs were constructed with the published *in vivo* data from nineteen different regions of the macaque cranium (Fig. 2). The mean of experimental averages from *in vivo* shear strain is depicted by the dotted black line and the dispersion (maximum range defined by the means$\pm$two standard deviations for each experiment) is depicted by the gray areas. Maximum shear strains were calculated from the finite element model at each site using strain data extracted in terms of 34 site—specific local *xyz* coordinate systems. Each local coordinate system had its origin at the node located at the center of each strain gage location and its *xy* plane laid tangent to the surface of the cranium. Maximum shear strain at the site was calculated using the formula:

$$\gamma_{max} = \sqrt{(\epsilon_x - \epsilon_y)^2 + \gamma_{xy}^2} \quad (2)$$

where x, y, and z are coordinates of the site-specific coordinate system and ε_x, ε_y, and γ_{xy} are normal strain in the x-direction, normal strain in the y-direction, and the engineering shear strain1 in the xy plane, respectively. This enabled the maximum shear strain in the plane of the surface to be calculated and any contributions to maximum shear strain due to out-of-plane strains to be discarded. This was necessary since strains measured by strain gages in the *in vivo* experiments do not account for any strain components involving the direction normal to the plane of the strain gage.

2.4. The models

2.4.1. Models 1 and 2: simple isotropic material properties

In models 1 and 2 (see Table 1 for model descriptions) the macaque cranium was divided into three distinct materials – trabecular bone, cortical bone, and teeth – consisting of isotropic material properties (Table 2). In model 1 the input variables were randomized with a CV of 0.2 and a Gaussian distribution. In model 2 the input variables were randomized with their experimentally determined standard deviations and a Gaussian distribution (Wang and Dechow, 2006).

2.4.2. Models 3 and 4: regional isotropic material properties

In models 3 and 4 the cranium was divided into 35 distinct regions, increasing non-homogeneity from models 1 and 2. Each region was assigned its own distinct set of isotropic material properties which are defined in Table 3. Similar to models 1 and 2, material properties were randomized with a CV of 20% and a Gaussian distribution in model 3 and all the material properties were randomized with their experimentally determined standard deviations and a Gaussian distribution in model 4.

2.4.3. Models 5 and 6: regional orthotropic material properties

For models 5 and 6, the macaque cranium was divided into the same regions as in Models 3 and 4. However, each region was assigned its own set of orthotropic material properties, thus increasing anisotropy. Exceptions to this were the teeth, trabecular bone, nasal septum, and neural and basicranial regions, which were modeled isotropically as in models 3 and 4. The orthotropic material properties are given in Table 4. Similar to models 3 and 4, material properties were randomized with a CV of 20% and a Gaussian distribution in model 5 and all the material properties were randomized with their experimentally determined standard deviations and a Gaussian distribution in model 6.

When the material properties were experimentally determined (Wang and Dechow, 2006), the nomenclature was standardized such that $E_3 > E_2 > E_1$, $G_{13} > G_{23} > G_{12}$, and $\nu_{12} > \nu_{23} > \nu_{13}$. In general, the material properties tend to be positively correlated to one another, so a larger E_3 tends to result in a larger E_2 and E_1. There exists no exact mathematical function that defines the relationships between each material property, so correlation coefficients relating the material properties to each other were calculated from empirical data (see Table 5). These correlation coefficients were specified in the ANSYS Probabilistic Design module.

2.4.4. All models

Comparisons of results between models 1 and 3 and models 2 and 4 provide two assessments of the effect of increasing non-homogeneity in the skull that has on the various biomechanical responses. Comparisons of results between models 3 and 5 and models 4 and 6 provide two assessments of the effect that increasing anisotropy in the skull has on various biomechanical responses. Finally, comparisons between models 1 and 2, 3 and 4, and 5 and 6 provide an assessment of the effect of assuming constant coefficient of variation for all material property values, versus using coefficients of variations gleaned from experimental data.

For models 1, 3, and 5, the coefficients of variation were calculated at sampling locations with modest-to-high magnitude principal compressive, principal tensile, and von Mises stresses and strains (Table 6 and Fig. 3). ("Modest-to-high magnitude" means strains with a magnitude greater than 250 $\mu\varepsilon$ and stresses of greater than 3 MPa.) The coefficients of variation depict the magnitudes by which the averages and standard deviations of the stresses and strains at these various locations across the cranium were affected relative to each other when a 20% variation was applied to the material properties.

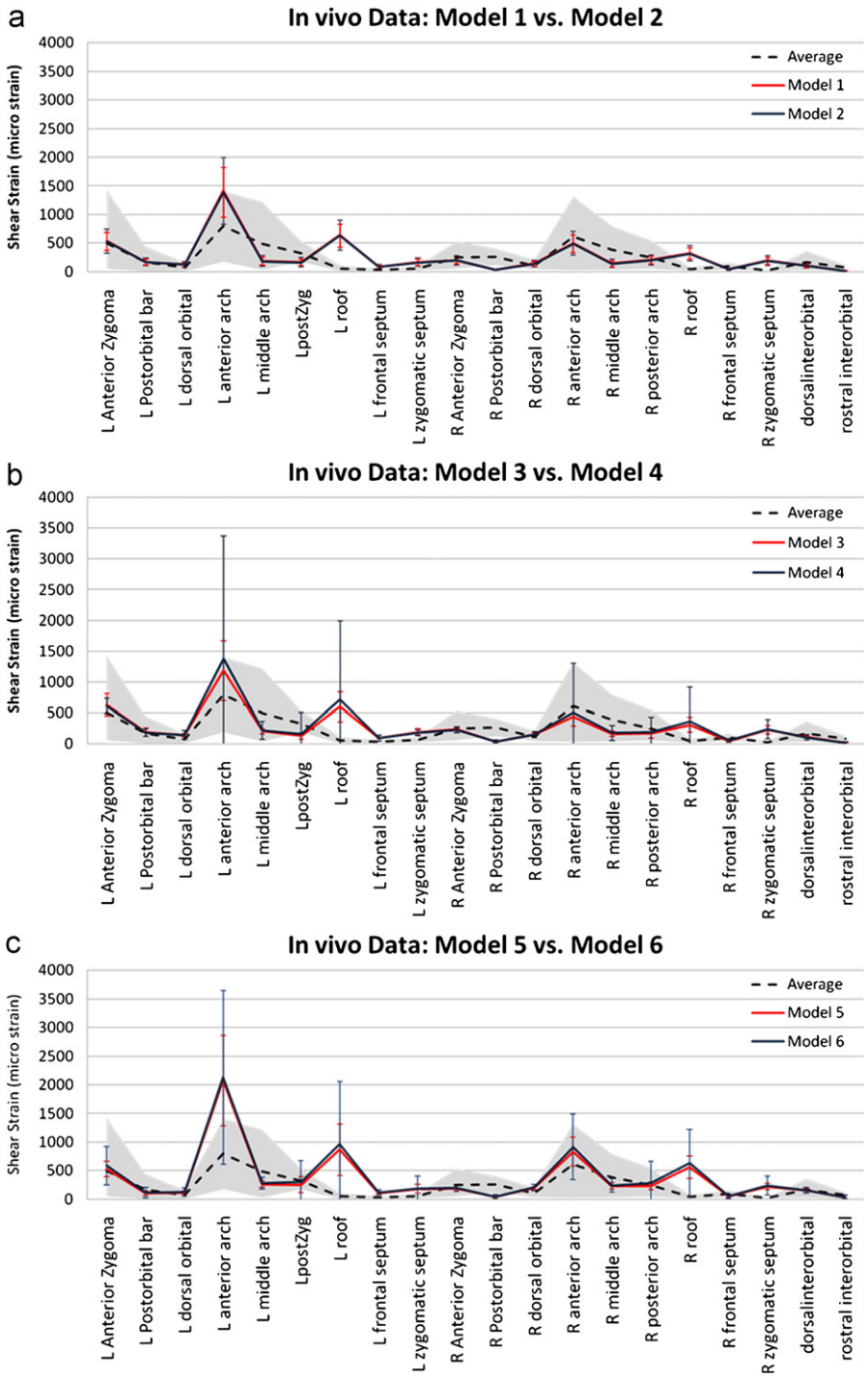

Fig. 2. Results from the probabilistic analyses compared to the in vivo data. The gray area depicts the dispersion of the *in vivo* data, and the error bars depict the 95% confidence interval (+/−2 standard deviations) of the shear strain at the various locations across the cranium (a) comparison between models 1 and 2 (3 region, isotropic material properties), (b) comparison between models 3 and 4 (multiple region, isotropic material properties), and (c) comparison between models 5 and 6 (multiple region, orthotropic).

3. Results

3.1. Models 1, 3, and 5

Models 1, 3, and 5 provide a unique opportunity to see how variability in stresses and strains are affected by non-homogeneity and anisotropy when standard variability in material properties is applied.

In model 1, the principal and von Mises strains are significantly more affected by variation in material properties than are the principal and von Mises stresses, as is seen by the larger coefficients of variation for the strains (see Table 6 and Fig. 3). As the material properties vary with a coefficient of variation of 0.2, modest-to-high magnitude strains vary consistently with an average coefficient of variation of 0.210, whereas the modest-to-high magnitude stresses vary consistently with a coefficient of variation of only 0.016.

Table 2
Mean material property values used for models 1 and 2 (three region isotropic). The standard deviations in the table were used to randomize the material properties in model 2; a CV of 0.2 was used to randomize the mean values of the material properties for model 1.

Region	Modulus of elasticity (MPa)		Poisson's ratio	
	Avg.	Standard deviation	Avg.	Standard deviation
Cortical bone	17,060	2760	0.28	0.10
Teeth	70,000	14,000	0.30	0.06
Trabecular bone	637	127	0.28	0.056

Table 3
Mean material property values used for models 3 and 4 (multiple region isotropic). The standard deviations in the table were used to randomize the material properties in model 4; a CV of 0.2 was used to randomize the mean values of the material properties for model 3.

Region	Modulus of elasticity (MPa)		Poisson's ratio	
	Avg.	Standard deviation	Avg.	Standard deviation
Premaxilla	18,500	1700	0.18	0.07
P3–M1 alveolus	16,700	3000	0.24	0.13
M2–M3 alveolus	20,600	4400	0.24	0.07
Anterior palate	15,300	4200	0.36	0.11
Posterior palate	18,800	7900	0.26	0.17
Dorsal rostrum	19,900	3100	0.21	0.13
Lateral rostrum	18,100	5400	0.24	0.09
Root of zygoma	17,900	3000	0.30	0.06
Anterior zygomatic arch	20,800	8300	0.28	0.12
Posterior zygomatic arch	12,500	900	0.27	0.20
Medial orbital wall	14,600	8900	0.40	0.11
Postorbital bar	19,800	8200	0.22	0.14
Frontal torus	13,100	4200	0.24	0.18
Glabella	14,400	2900	0.14	0.10
Frontal squama	14,900	7800	0.27	0.14
Neuro- and basicrania	17,300	5000	0.28	0.14
Septum	13,194	3800	0.28	0.14
Teeth	70,000	20,300	0.30	0.15
Trab bone	637	185	0.28	0.14

As non-homogeneity increases from model 1 to 3 (see Fig. 4), variation in the strains decreases from 0.210 to 0.180, but the variation in strains is less consistent, as is denoted by the increase in the standard deviation of the coefficients of variation from 0.007 to 0.047. Variation in the stresses, however, increases greatly from 0.016 to 0.106, and like the strains, the variation in stresses is less consistent in model 3 than in model 1.

Finally, as anisotropy increases from model 3 to 5 (see Fig. 5), variation in both the stresses and strains decreases.

3.2. Models 2, 4, and 6

In model 2 the strains vary consistently with a coefficient of variation of 0.165 while the stresses vary consistently at a lower level of 0.025. As non-homogeneity increases from model 2 to 4 (see Fig. 4), the level of variation in strains increases greatly from 0.165 to 0.560 and the strains vary much less consistently. The level of variation in the stresses also increases and the stresses vary less consistently, but not to the level of variation in the strains (see Table 6).

As anisotropy increases (see Fig. 5), the average coefficient of variation in the strains decreases to 0.369 and the strains vary more consistently than they did in model 2. However, the levels of variation are still very inconsistent (meaning the coefficients of variation have a large standard deviation), indicated by the average coefficients of variation, which have a standard deviation of 0.183. The variation in stresses again increases, this time to 0.150, but the stresses vary more consistently.

3.3. Comparing the models to in vivo data

Results from the probabilistic analyses are compared to the *in vivo* data in Fig. 4. When validating a craniofacial FE model, validation is typically achieved by comparing strains on the model to *in vivo* or *ex vivo* strain data. Ideally, the *in vivo* or *ex vivo* data would have come from the same individual who was used to create the FE model, and the material properties and muscle forces applied to the FE model would have been taken from that same individual as well. Validation of the models was considered to be good at most locations on the cranium (where

Table 4
Mean material property values used for models 5 and 6 (multiple region orthotropic). The standard deviations in the table were used to randomize the material properties in model 6; a CV of 0.2 was used to randomize the mean values of the material properties for model 5. The teeth, trabecular bone, septum, and neuro- and basicranium were all given the isotropic material properties assigned in models 3 and 4 for both models 5 and 6.

Region	Modulus of elasticity (MPa)						Shear modulus (MPa)						Poisson's ratio					
	*E*1		*E*2		*E*3		*G*12		*G*23		*G*13		*v*12		*v*23		*v*13	
	Avg.	Std. dev.	Avg.	Std. dev.	Avg.	Std. dev.	Avg.	Std. dev.	Avg.	Std. dev.	Avg.	Std. dev.	Avg.	Std. dev.	Avg.	Std. dev.	Avg.	Std. dev.
Premaxilla	10,000	1400	13,900	3900	18,500	1700	4400	1100	5200	1000	7300	1900	0.29	0.16	0.18	0.07	0.15	0.15
P3M1 alveolus	9900	3900	12,100	4000	16,700	3000	4300	1700	5800	2400	7400	2100	0.33	0.21	0.24	0.13	0.17	0.11
M2M3 alveolus	12,600	3900	15,400	4000	20,600	4400	4900	1500	6400	2400	7900	2600	0.35	0.13	0.24	0.07	0.22	0.16
Anterior palate	7500	1400	8800	1500	15,300	4200	2600	400	2800	400	3600	900	0.41	0.06	0.36	0.11	0.26	0.11
Posterior palate	6400	1000	7500	1500	18,800	7900	2200	400	2500	400	3300	900	0.48	0.08	0.26	0.17	0.23	0.13
Dorsal rostrum	12,200	2100	14,000	2100	19,900	3100	5000	900	6900	1800	8900	2900	0.32	0.14	0.21	0.13	0.14	0.06
Lateral rostrum	11,500	5300	14,400	5400	18,100	5400	4700	2500	5300	2100	7300	3100	0.37	0.13	0.24	0.09	0.15	0.13
Root of zyg. arch	8900	2900	10,900	4400	17,900	3000	3700	1700	5300	1200	8600	3300	0.53	0.15	0.3	0.06	0.18	0.12
Anterior zyg. arch	8600	4700	12,400	5700	20,800	8300	4200	1900	4600	1500	8600	2800	0.39	0.19	0.28	0.12	0.22	0.17
Posterior zyg. arch	8200	2700	10,000	2900	12,500	900	3100	1100	3800	1100	4900	1600	0.34	0.10	0.27	0.20	0.24	0.19
Med orbital wall	7100	4400	11,500	6500	14,600	8900	3600	2000	4200	2400	9000	5900	0.46	0.12	0.40	0.11	0.23	0.16
Postorbital bar	11,300	3600	13,100	3300	19,800	8200	4400	1500	6400	2200	8000	2500	0.44	0.07	0.22	0.14	0.15	0.13
Frontal torus	10,200	2900	11,200	3100	13,100	4200	4300	1400	5100	1900	6000	1800	0.32	0.20	0.24	0.18	0.19	0.08
Glabella	9200	2300	9700	2100	14,400	2900	3300	900	4800	1400	5100	1200	0.46	0.08	0.14	0.10	0.21	0.09
Frontal squama	7900	3800	11,000	5000	14,900	7800	3400	1500	4300	2300	7100	3500	0.49	0.12	0.27	0.14	0.18	0.18

Table 5
Coefficients of correlation (R) for orthotropic material properties, calculated using data taken from Wang and Dechow (2006). E_1/E_2 represents the coefficient of correlation between E_1 and E_2, G_{12}/G_{31} the coefficient of correlation between G_{12} and G_{31}, etc.

Region	E_1/E_2	E_2/E_3	E_1/E_3	G_{12}/G_{31}	G_{31}/G_{23}	G_{12}/G_{23}	ν_{12}/ν_{13}	ν_{13}/ν_{23}	ν_{12}/ν_{13}
Vault	0.900	0.910	0.830	0.829	0.579	0.529	0.273	0.423	0.440
Circumorbital	0.916	0.903	0.796	0.816	0.685	0.807	0.412	0.530	0.465
Zygomatic arch	0.904	0.881	0.801	0.747	0.545	0.687	0.642	0.512	0.279
Muzzle	0.933	0.925	0.946	0.681	0.319	0.312	0.600	0.383	0.708
Alveolus	0.564	0.724	0.579	0.798	0.564	0.402	0.177	0.283	0.306
Intraorbital	0.915	0.909	0.883	0.918	0.563	0.608	0.146	0.665	0.094
Palatine	0.704	0.585	0.159	0.889	0.439	0.623	0.842	0.208	0.328

Table 6
The coefficients of variation for the minimum and maximum principal and von Mises stresses and strains were calculated for modest-to-high magnitude stresses (greater than 3 MPa) and microstrains (greater than 250 $\mu\varepsilon$) at each of the 34 sites across the cranium. The coefficients of variation were averaged and the standard deviations were calculated to convey the magnitude to which the stresses and strains varied at the various sites across the cranium and how predictable this level of variation is.

	Model	Average coefficients of variation	
		Strains	Stresses
Input variables with CV=0.2	(1) 3 Region, isotropic	0.210 ± 0.007	0.016 ± 0.009
	(3) Multiple regions, isotropic	0.169 ± 0.028	0.104 ± 0.043
	(5) Multiple regions, orthotropic	0.144 ± 0.042	0.081 ± 0.025
Input variables with standard deviations based on empirical data	(2) 3 Region, isotropic	0.165 ± 0.011	0.025 ± 0.017
	(4) Multiple regions, isotropic	0.560 ± 0.334	0.124 ± 0.043
	(6) Multiple regions, orthotropic	0.369 ± 0.183	0.150 ± 0.038

the FEA results fell within the experimental range) but poor in some locations (i.e. the left and right orbital roofs). As non-homogeneity and anisotropy increased from models 1 and 2 to models 3 and 4 to models 5 and 6 (see Figs. 4 and 5), the FEA results $+/-2$ standard deviations include or nearly include the average from the *in vivo* data. When the cranium is modeled with the highest level of simplicity (model 1, where anisotropy and non-homogeneity are low and no empirical data is used to calculate the standard deviations) the average *in vivo* shear strain is within the range or nearly within the range of the FEA results for only 10 out of the 20 locations. However, when the macaque cranium is modeled with the highest level of accuracy (model 6), the average *in vivo* shear strain is within or nearly within the range of the FEA results for 18 out of the 20 locations.

This implies that model 6 is a more realistic model than model 1, and that modeling with a higher level of accuracy will give the modeler a better chance of having *in silico* results that will match the *in vivo* results. This also implies that when modeling simplistically, a model that appears to be invalid could actually be valid when uncertainty in material properties is accounted for.

When empirical data are used to calculate the CVs for material properties and the cranium is modeled simplistically (model 2), the variability in the shear strains is minimal. A large number of the average shear strains also fall within the dispersion of the *in vivo* data. As non-homogeneity increases (model 4), the magnitude of the shear strains remains consistent but the variability in the shear strains increases greatly. Finally, as anisotropy increases (model 6), the magnitude of the shear strains changes at multiple locations across the cranium and the variability in the shear strains increases.

When comparing the variability in the *in vivo* data to the variability in the FEA results, the variability in the FEA results puts a lower bound on the total variability of *in vivo* data, assuming variability in the *in vivo* data due to muscle forces, morphology, and material properties are all independent. Considering that there are some locations where the variability in the FEA results exceeds the variability in the *in vivo* data, this could imply there is an error with the data set, an error with the model, or that the assumption that variability in muscle forces, morphology, and materials properties are independent could be false, i.e. muscles forces, morphology, and material properties could be positively correlated.

4. Discussion

4.1. Comparing models 1, 3, and 5 and models 2, 4, and 6

In all cases when a coefficient of variation of 0.2 is applied to the material properties (models 1, 3, and 5), there is less variability in the shear strain than when a coefficient of variation calculated from empirical data is applied. Therefore, applying a coefficient of variation of 0.2 to the material properties underestimates the variability in the shear strains across the cranium in the FE model. This conclusion is further supported by the results in Table 6 and Fig. 3, where the variability in the minimum and maximum principal and von Mises stresses and strains is always lower when a coefficient of variation of 0.2 is applied to the material properties compared to when a coefficient of variation calculated from empirical data is applied. When the cranium is modeled most simply, i.e. consisting of three isotropic homogeneous materials (models 1 and 2), the variability in the moderate-to-high minimum and maximum principal and von Mises stresses and strains are less than when the cranium is modeled with the highest level of accuracy (see models 5 and 6 in Table 6 and Fig. 3). Therefore, it should be understood that when the cranium is modeled as consisting of three homogeneous isotropic materials, the level of variability due to uncertainty in material property values in the stresses and strains is minimized. When the cranium is modeled with greater material complexity by reducing the level of homogeneity (model 4), the accuracy of the model remains the same but the level of variability in stresses and strains due to uncertainty in material property values increases (Table 6 and Fig. 3).

Models 2, 4, and 6 show that when the variation in material properties is known, variability in both stresses and strains increases greatly as non-homogeneity and anisotropy increase.

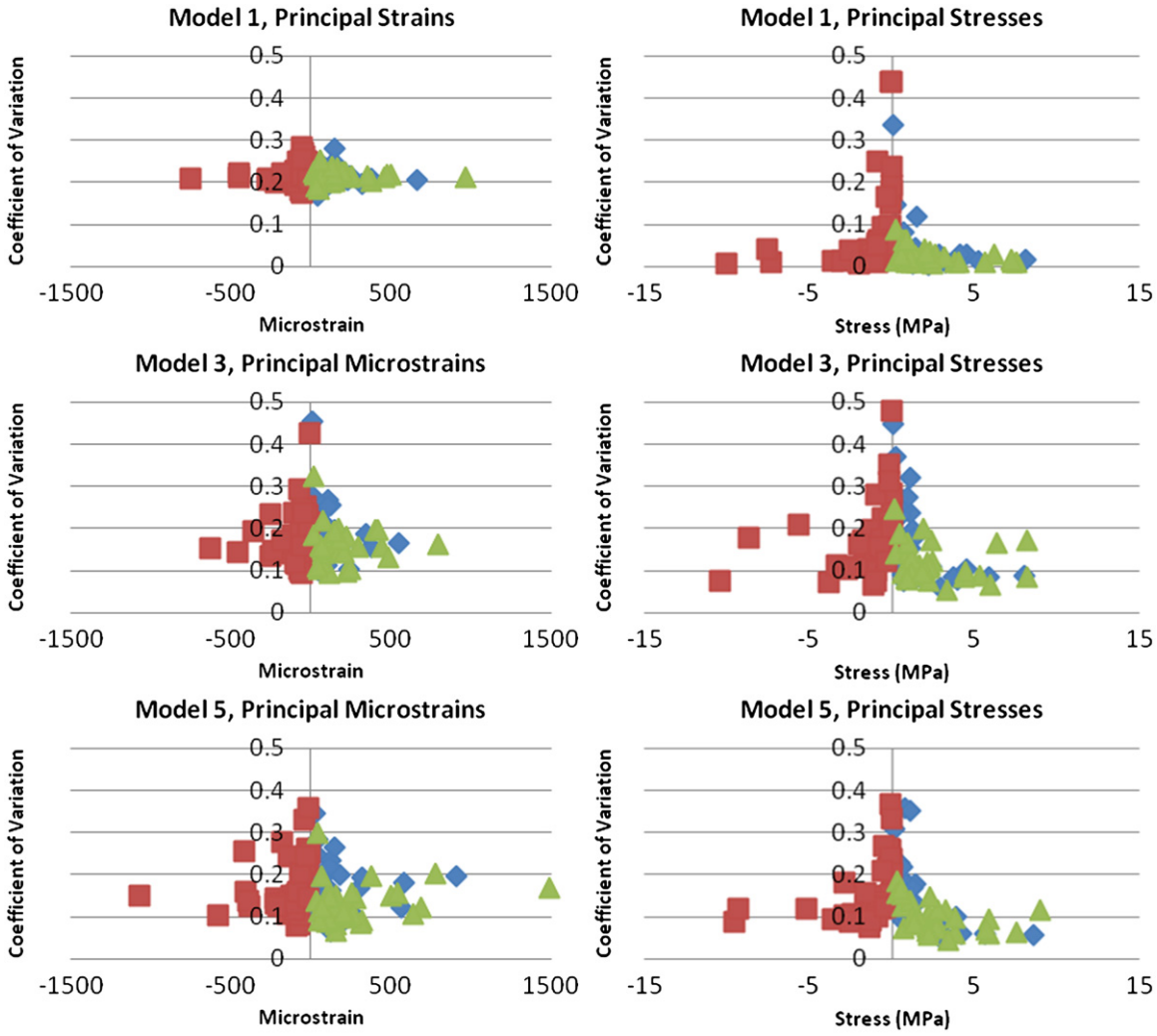

Fig. 3. Coefficients of variation plotted against the average microstrains and stresses for models 1, 3, and 5. The average coefficient of variation for the modest-to-high magnitude microstrains and stresses (microstrains greater than 250 and stresses greater than 3 MPa) can be found in Table 6. The blue diamonds represent tensile strains/stresses, the red squares represent the compressive strains/stresses, and the green triangles represent von Mises strains/stresses. (For interpretation of the references to color in this figure legend, the reader is referred to the web version of this article.)

4.2. Testing the hypotheses

The first hypothesis, that uncertainty in material property values will have little effect on high stresses and a large effect in high strains for homogeneous isotropic models, is fully supported by models 1 and 2, as seen by the average coefficients of variation reported in Table 5. For model 1 in which isotropic material properties were randomized with CV=0.2, the average CV for all stress measures at all sampling sites is only 0.016, whereas the average coefficient of variation for modest to high strains measures 0.210. In model 3, which used CVs of isotropic material property values based on empirical data, the average CV for stress was 0.025 and the average CV for strain was 0.16.

The second hypothesis is supported by the probabilistic analysis results since, as non-homogeneity and anisotropy increase, the CV for modest-to-high magnitude stresses increases (see Table 6). The third hypothesis may be supported through the results of this experiment. The error bars in Fig. 2 depict a 95% confidence interval calculated from the probabilistic analyses. All models have a large 95% confidence interval, which supports the conclusion that variation in material properties causes significant variation in maximum shear strain on the surface of the cranium. Therefore, since the *in vivo* data were gathered from multiple individuals, some of the variation in the data could be due to variation in material properties and/or geometry of the cortical bone between individuals.

When the material properties were varied with standard deviations calculated from empirical data, the level of variation in modest-to-high magnitude stresses and strains differs greatly from when a 20% variation is applied to the material properties. Models 1, 3, and 5 suggest that, if all material property values of a system have about the same level of randomness, variability in material property values causes variability in principal stresses to increase and variability in principal strains to decrease as non-homogeneity and anisotropy increase. However, the variability in material property values is not constant in macaque crania. Since the trends in variability in the stresses and strains differ from models 1, 3, and 5 to models 2, 4, and 6 (see Table 6), this leads us to conclude that the assumption of constant material property variability produces inaccurate trends in variability in stresses and strains with respect to how the skull is modeled in terms of homogeneity and anisotropy.

Therefore, if a probabilistic analysis is to be carried out to determine how variability in the material properties of bone affect stress and strain, a knowledge of the actual biological variability in material property values is required. This nullifies

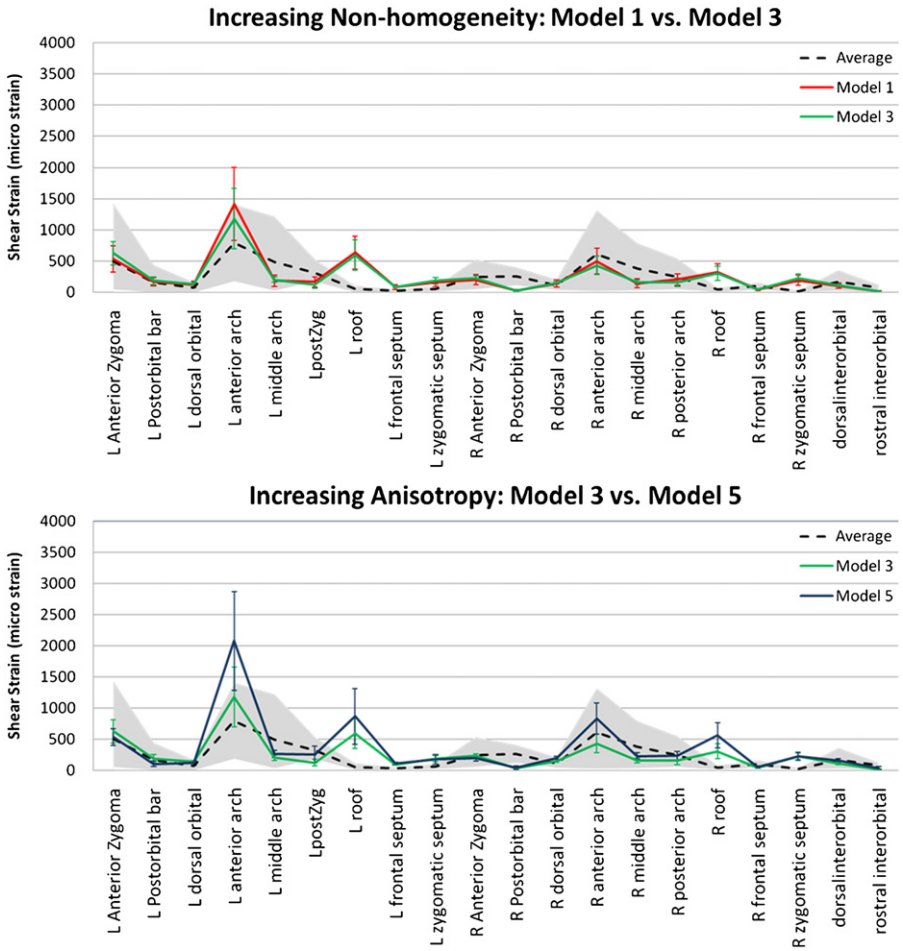

Fig. 4. *In vivo* data plotted against simulation results depicting how shear strain varies as non-homogeneity increases from model 1 to 3 and from model 2 to 4.

the fourth hypothesis, and implies that if such knowledge of the variability in material property values is not known, trends in variability in stresses and strains cannot be trusted as being correct.

5. Conclusion

Ideally, an FE model of an individual's cranium would be constructed in which information pertaining to the material properties and muscle forces of that individual's cranium were previously gathered, and in which *in vivo* or *ex vivo* data on that individual that could be used to validate the model. However, in practice this standard is difficult to achieve, and therefore an understanding of how much variation in FE model results is due to lack of accurate individual-specific data is needed. Our results indicate that large variations in modest-to-high strains and lower variations in modest-to-high stresses occur due to variation in material property values. More work is needed to quantify how variation in morphology between individuals and variation in loads (due to both intra and inter-individual variation) affect moderate-to-high stresses and strains in craniofacial FE models.

Also, the high sensitivity of modest-to-high strain versus the low sensitivity of modest-to-high stresses due to randomness in material property values across individuals may have implications in terms of bone remodeling. It is generally accepted that bone remodeling occurs as a results of deformations that occur at a microstructural level (Burra et al., 2010; Bonivtch et al., 2007; You et al., 2001; Cowin, 1999; Cowin et al., 1995; Pavalko et al., 2003). To date, there is no consensus as to what macroscopic mechanics quantities are correlated with these deformations. If microstructural deformations and bone remodeling are correlated to strain, then one would expect bone remodeling to be highly sensitive to variation in material properties, since such variability causes a large level of variation in moderate-to-high microstrains. If cellular deformations are correlated to stress, then one would expect bone remodeling to be fairly insensitive to variations in material properties, since we found moderate-to-high stress to have relatively low variation due to variation in material property values.

Of course, stress and strain are continuum mechanics concepts, and the current investigation is focused on macro-level mechanics, while the actual mechanical signature to which bone responds is at the hierarchical level of the bone matrix that directly affects cellular response (You et al., 2001; Cowin, 1999; Cowin et al., 1995; Pavalko et al., 2003). However, little is known about variation in microscale material properties in bone tissues in three dimensions and how this variation may affect cellular response.

Finally, we note that our data suggest that it is incorrect to assume that variability in muscle forces, morphology, materials properties, and other "cranial variables" are independent (the error bars for the *in silico* results in Fig. 2 cover a much larger spread than the error bars for the *in vivo* results). The fact that positive correlations between these quantities would result in less variability in stress and strain than if these quantities were independent has evolutionary implications. Evolution could be producing a robust system—one whose mechanical performance

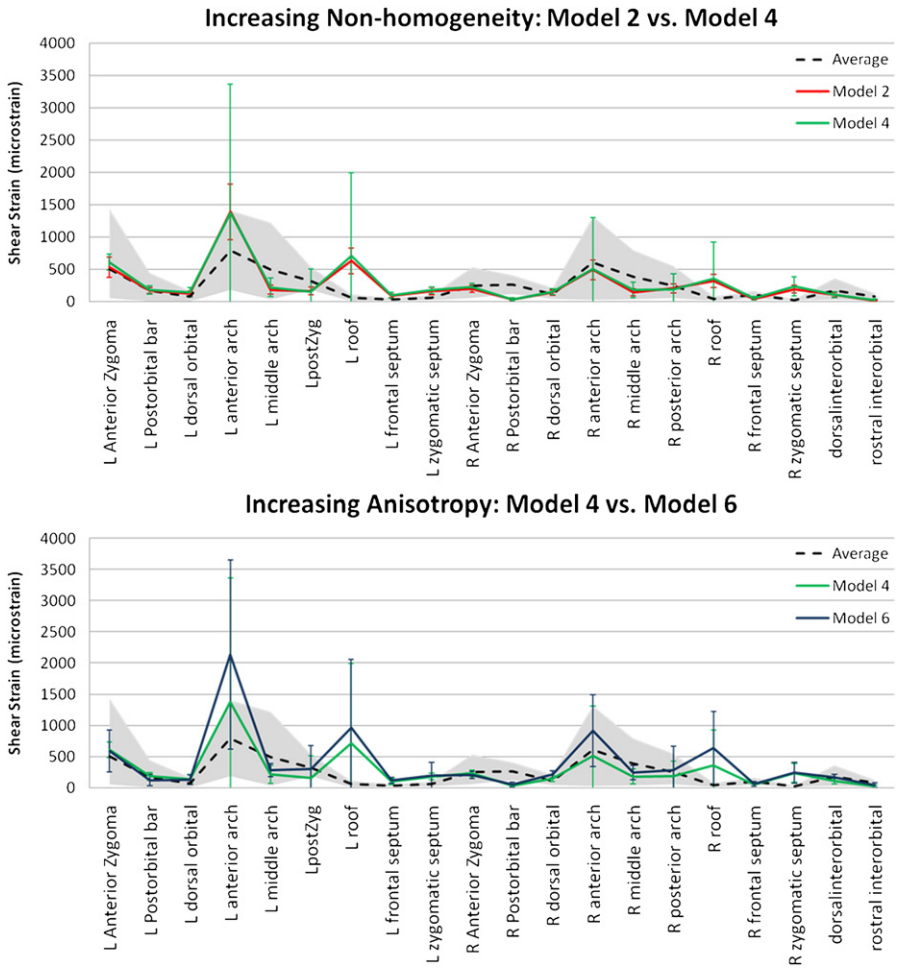

Fig. 5. In vivo data plotted against simulation data depicting how shear strain varies as anisotropy increases from model 3 to 5 and from model 4 to 6.

is relatively insensitive to variations or uncertainty in its inputs—by developing positively correlated cranial variables which reduce variability in shear strains during cranial function. If this holistic view of cranial variables affecting mechanical performance is correct, one might hypothesize that many of the biomechanical variables in the cranium would evolve together.

Acknowledgments

We thank Professor Betsy Dumont and members of the University of Massachusetts Mammology Lab for their help and input in reviewing this paper. This work is supported by the National Science Foundation Physical Anthropology HOMINID program (BCS 0725126, 0725147, BCS 0725078, 0725183, and 0725141) and the National Science Foundation Biomesh Grant (DBI 0743460). NSF was not involved in this research.

References

Berthaume, M., Grosse, I.R., Patel, N.D., Strait, D.S., Wood, S., Richmond, B.G., 2010. The effect of early hominin occlusal morphology on the fracturing of hard food items. Anat. Rec.: Adv. Integrative Anat. Evol. Biol. 293, 594–606.

Brekelmans, W., Poort, H., Slooff, T., 1972. A new method to analyse the mechanical behaviour of skeletal parts. Acta Orthop. Scand. 43, 301.

Burra, S., Nicolella, D.P., Francis, W.L., Freitas, C.J., Mueschke, N.J., Poole, K.J., Jiang, J.X., 2010. Dendritic processes of osteocytes are mechanotransducers that induce the opening of hemichannels. PNAS 107, 13648–13653.

Bonivtch, A.R., Bonewald, L.F., Nicolella, D.P., 2007. Tissue strain amplification at the osteocyte lacuna: a microstructural finite element analysis. J. Biomech. 40, 2199–2206.

Cesare, M.A., Sues, R.H., 1999. Profes Probabilistic Finite Element Analysis—Bringing Probabilistic Mechanics to the Desktop. AIAA, pp. 1–11.

Chamoli, U., Wroe, S., 2011. Allometry in the distribution of material properties and geometry of the felid skull: why larger species may need to change and how they may achieve it. J. Theor. Biol. 283, 217–226.

Cowin, S.C., 1999. Bone poroelasticity. J. Biomech. 32, 217–238.

Cowin, S.C., Weinbaum, S., Zeng, Y., 1995. A case for bone canaliculi as the anatomical site of strain generated potentials. J. Biomech. 28, 1281–1297.

Dumont, E.R., Ryan, T.M., Godfrey, L.R., 2011. The *Hadropithecus conundrum* reconsidered, with implications for interpreting diet in fossil hominins. Proc. R. Soc. B: Biol. Sci.

Davis, J.L., Dumont, E.R., Strait, D.S., Grosse, I.R., 2011. An efficient method of modeling material properties using a thermal diffusion analogy: an example based on craniofacial bone. PLoS ONE 6 (2), e17004. doi:10.1371/journal.pone.0017004.

Dumont, E.R., Piccirillo, J., Grosse, I.R., 2005. Finite-element analysis of biting behavior and bone stress in the facial skeletons of bats. Anat. Rec. Part A: Discoveries Mol. Cell. Evol. Biol. 283A, 319–330.

Der Kiureghian, A., Ke, J., 1988. The stochastic finite element method in structural reliability. Prob. Eng. Mech 3, 83–91.

Grine, F.E., Judex, S., Daegling, D.J., Ozcivici, E., Ungar, P.S., Teaford, M.F., Sponheimer, M., Scott, J., Scott, R.S., Walker, A., 2010. Craniofacial biomechanics and functional and dietary inferences in hominin paleontology. J. Hum. Evol. 58, 293–308.

Hecht, E.M., Cullinane, D.M., Grosse, I.R., 2010. A novel stress distribution organ in the arthropod exoskeleton. Arthropod Struct. Dev. 39, 305–309.

Hueste, M.B.D., Chompreda, P., Trejo, D., Cline, D.B.H., Keating, P.B., 2004. Mechanical properties of high-strength concrete for prestressed members. ACI Struct. J., 457–465.

Hylander, W.L., Johnson, K.R., 1994. Jaw muscle function and wishboning of the mandible during mastication in macaques and baboons. Am. J. Phys. Anthropol. 94, 523–547.

Kotha, S.P., Hsieh, Y.-, Strigel, R.M., Müller, R., Silva, M.J., 2004. Experimental and finite element analysis of the rat ulnar loading model—correlations between strain and bone formation following fatigue loading. J. Biomech. 37, 541–548.
Kang, Z., 2005. Robust Design Optimization of Structures Under Uncertainties.
Kupczik, K., Dobson, C.A., Fagan, M.J., Crompton, R.H., Oxnard, C.E., Higgins, P.O, 2007. Assessing mechanical function of the zygomatic region in macaques: validation and sensitivity testing of finite element models. J. Anat. 210, 41–53.
Leysen, H., Jouk, P., Brunain, M., Christiaens, J., Adriaens, D., 2010. Cranial architecture of tube-snouted gasterosteiformes (*Syngnathus rostellatus* and *Hippocampus capensis*). J. Morphol. 271, 255–270.
Lewis, E.E., 1987. Introduction to Reliability Engineering. Wiley, New York.
Metzger, K.A., Daniel, W.J.T., Ross, C.F., 2005. Comparison of beam theory and finite-element analysis with in vivo bone strain data from the alligator cranium. Anat. Rec. Part A: Discoveries Mol. Cell. Evol. Biol. 283A, 331–348.
Melchers, R.E., 1987. Structural Reliability: Analysis and Prediction. Horwood, New York, NY.
Malvern, L.E., 1969. Introduction to the Mechanics of a Continuous Medium.
McElhaney, J.H., Fogle, J.L., Melvin, J.W., Haynes, R.R., Roberts, V.L., Alem, N.M., 1970. Mechanical properties of cranial bone. J. Biomech. 3. (pp. 495–496, 497–511, IN5).
Nicolella, D.P., Thacker, B.H., Katoozian, H., Davy, D.T., 2001. Probabilistic risk analysis of a cemented hip implant. J. Math. Modeling Sci. Comput. 13, 98.
O'Higgins, P., Cobb, S.N., Fitton, L.C., Gröning, F., Phillips, R., Liu, J., Fagan, M.J., 2011. Combining geometric morphometrics and functional simulation: an emerging toolkit for virtual functional analyses. J. Anat. 218, 3–15.
Olsson, A.M.J., Sandberg, G.E., 2002. Latin hypercube sampling for stochastic finite element analysis. J. Eng. Mech. 128.
Porro, L.B., Holliday, C.M., Anapol, F., Ontiveros, L.C., Ontiveros, L.T., Ross, C.F., 2011. Free body analysis, beam mechanics, and finite element modeling of the mandible of *Alligator mississippiensis*. J. Morphol.
Peterson, J., Dechow, P.C., 2003. Material properties of the human cranial vault and zygoma. Anat. Rec. Part A: Discoveries Mol. Cell. Evol. Biol. 274A, 785–797.
Pavalko, F.M., Norvell, S.M., Burr, D.B., Turner, C.H., Duncan, R.L., Bidwell, J.P., 2003. A Model for mechanotransduction in bone cells: the load-bearing mechanosomes. J. Cell. Biochem. 88, 104–112.
Ross, C.F., Berthaume, M.A., Dechow, P.C., Iriarte-Diaz, J., Porro, L.B., Richmond, B.G., Spencer, M., Strait, D., 2011. In vivo bone strain and finite-element modeling of the craniofacial haft in catarrhine primates. J. Anat. 218, 112–141.
Rayfield, E.J., 2007. Finite element analysis and understanding the biomechanics and evolution of living and fossil organisms. Annu. Rev. Earth Planet. Sci. 35, 541–576.
Ross, C.F., Patel, B.A., Slice, D.E., Strait, D.S., Dechow, P.C., Richmond, B.G., Spencer, M.A., 2005. Modeling masticatory muscle force in finite element analysis: sensitivity analysis using principal coordinates analysis. Anat. Rec. Part A: Discoveries Mol. Cell. Evol. Biol. 283A, 288–299.
Rybicki, E.F., Simonen, F.A., Weis Jr, E.B., 1972. On the mathematical analysis of stress in the human femur. J. Biomech. 5, 203–215.
Rayfield, E.J., 2004. Cranial mechanics and feeding in *Tyrannosaurus rex*. Proc. R. Soc. London Ser. B: Biol. Sci. 271, 1451–1459.
Reed, D.A., Porro, L.B., Iriarte-Diaz, J., Lemberg, J.B., Holliday, C.M., Anapol, F., Ross, C.F., 2011. The impact of bone and suture material properties on mandibular function in *Alligator mississippiensis*: testing theoretical phenotypes with finite element analysis. J. Anat. 218, 59–74.
Rayfield, E.J., 2005. Using finite-element analysis to investigate suture morphology: a case study using large carnivorous dinosaurs. Anat. Rec. Part A: Discoveries Mol. Cell. Evol. Biol. 283A, 349–365.
Reh, S., Beley, J., Mukherjee, S., Khor, E.H., 2006. Probabilistic finite element analysis using ANSYS. Struct. Saf. 28, 17–43.
Strait, D.S., Wang, Q., Dechow, P.C., Ross, C.F., Richmond, B.G., Spencer, M.A., Patel, B.A., 2005. Modeling elastic properties in finite-element analysis: how much precision is needed to produce an accurate model? Anat. Rec. Part A: Discoveries Mol. Cell. Evol. Biol. 283A, 275–287.
Sudret, B., der Kiureghian, A., 2000. Stochastic Finite Element Methods and Reliability: A State-of-the-Art Report. Technical Report UCB/SEMM-2000/08. Department of Civil & Environmental Engineering, University of California, Berkeley, CA.
Thacker, B.H., Nicolella, D.P., Kumaresan, S., Yoganandan, N., Pintar, F.A., 2000. Probabilistic finite element analysis of the human lower cervical spine. J. Math. Modeling Sci. Comput. 13, 12–21.
Timoshenko, S.P., Goodier, J.N., 1970. Theory of Elasticity, 3rd ed. McGraw-Hill, New York.
Wood, S.A., Strait, D.S., Dumont, E.R., Ross, C.F., Grosse, I.R., 2011. The effects of modeling simplifications on craniofacial finite element models: the alveoli (tooth sockets) and periodontal ligaments. J. Biomech., 44, 1831–1838.
Wroe, S., Huber, D.R., Lowry, M., McHenry, C., Moreno, K., Clausen, P., Ferrara, T.L., Cunningham, E., Dean, M.N., Summers, A.P., 2008. Three-dimensional computer analysis of white shark jaw mechanics: how hard can a great white bite? J. Zool. 276, 336–342.
Wang, Q., Dechow, P.C., 2006. Elastic properties of external cortical bone in the craniofacial skeleton of the rhesus monkey. Am. J Phys. Anthropol. 131, 402.
Wang, Q., Ashley, D.W., Dechow, P.C., 2010. Regional, ontogenetic, and sex-related variations in elastic properties of cortical bone in baboon mandibles. Am. J. Phys. Anthropol. 141, 526–549.
Wang, Q., Smith, A.L., Strait, D.S., Wright, B.W., Richmond, B.G., Grosse, I.R., Byron, C.D., Zapata, U., 2010. The global impact of sutures assessed in a finite element model of a macaque cranium. Anat. Rec.: Adv. Integrative Anat. Evol. Biol. 293, 1477–1491.
You, L., Cowin, S.C., Schaffler, M.B., Weinbaum, S., 2001. A model for strain amplification in the actin cytoskeleton of osteocytes due to fluid drag on pericellular matrix. J. Biomech. 34, 1375–1386.
Zapata, U., Metzger, K., Wang, Q., Elsey, R.M., Ross, C.F., Dechow, P.C., 2010. Material properties of mandibular cortical bone in the American alligator, *Alligator mississippiensis*. Bone 46, 860–867.